Peer-reviewed version available at Energies 2018, 11, 3062; doi:10.3390/en11113062

Article

High Gas Hydrate and Free Gas Concentrations: An Explanation for Seeps Offshore South Mocha Island

Iván Vargas-Cordero [1,*], Umberta Tinivella [2], Lucía Villar-Muñoz [3] and Joaquim P. Bento [4]

[1] Universidad Andres Bello (UNAB), Facultad de Ingeniería, Viña del Mar, Chile; ivan.vargas@unab.cl
[2] Istituto Nazionale di Oceanografia e di Geofisica Sperimentale (OGS), Trieste, Italy; utinivella@inogs.it
[3] Helmholtz Centre for Ocean Research (GEOMAR), Kiel, Germany; lucia.villar@gmail.com
[4] Escuela de Ciencias del Mar, Pontificia Universidad Católica de Valparaíso, Valparaíso, Chile; jnettojunior@gmail.com
* Correspondence: ivan.vargas@unab.cl; Tel.: +56-950598066

Abstract: Recent studies have reported shallow and deep seep areas offshore Mocha island. Gas hydrate occurrences along the Chilean margin could explain seeps presence. Gas phases (gas hydrate and free gas) and geothermal gradients were estimated analysing two seismic sections. Close to Mocha island (up to 20 km) were detected high (up to 1900 m/s) and low (1260 m/s) velocities associated with high gas hydrate (up to 20 % of total volume) and free gas (up to 1.1% of total volume) concentrations respectively. These values are in agreement with a variable and high geothermal gradient (65 to 110 °C/km) related to high supply deep fluids canalised by faults and fractures. Faraway from Mocha island (more than 60 km), free gas concentrations decrease to 0.3 % of total volume and low geothermal gradient (from 35 to 60 °C/km) are associated with low fluids supply. Finally, we propose gas hydrate dissociation processes as the main supply source for seeps in the vicinity of Mocha island. These processes can be triggered by ancient sliding reported in literature.

Keywords: gas hydrate; BSR; Mocha island.

1. Introduction

The studies regarding gas hydrate occurrences worldwide are important for three main reasons: a) energy resource; b) submarine geohazard and c) global climate change [1]. Gas hydrate distribution has been mapped mostly by using indirect measurements. From multichannel seismic data, it is possible to detect the principal indicator of gas hydrate presence known as bottom simulating reflector (BSR). The worldwide distribution of BSR occurs mainly in marine sediments along the active continental margins (predominantly circum-Pacific belt) and the permafrost regions (Antarctic and Arctic).

In Chile the interest for gas hydrate occurrences plays an important role due to the high seismicity that characterises the entire region. Several scientific studies have reported gas hydrate dissociation triggered by earthquakes e.g. Great Sumatra, Japan and Norwegian margins [2-6]. The BSR along the Chilean margin is recognized in the continental slope covering a wide extension close to 3000 km (from 33°S until 56°S). In this context, gas hydrate estimates contribute to evaluate submarine geohazards associated with gas hydrate dissociation and the potential methane reservoir. Moreover, the estimates of methane stored as gas hydrate and free gas phases in marine sediments can be used to model more realistic scenarios associated with gas hydrates dissociation and its effects as a greenhouse gas. Several studies along the Chilean margin have reported gas phases concentrations by modelling the seismic velocity [7-16] covering already 10% of the entire margin.

The present study add new information regarding gas phase concentrations southernwards offshore Mocha Island by using seismic and theoretical velocity models (Fig. 1). The Mocha island is characterised by active seismicity and constitutes an uplifted block during the Quaternary and emerged today in the Arauco peninsula [17,18]. Moreover, Mocha island is known by intertidal and

subtidal gas seepage system [19,20] and deeper seeps at 1400 water depth [21], whose presence probably is related to gas hydrates dissociation. In this context, gas phases estimates contribute to map and understand its role in fluid escapes supply.

In order to quantify gas phases a procedure already tested in previous studies is performed [11-16,22]. The method includes: a) Obtaining seismic velocity model by using Kirchhoff Pre-Stack Depth Migration (PSDM); b) Velocity anomalies evaluation; c) Gas phases estimates by fitting seismic velocity with theoretical velocity and d) Geothermal gradient calculation by using seafloor and BSR depths and water bottom temperature.

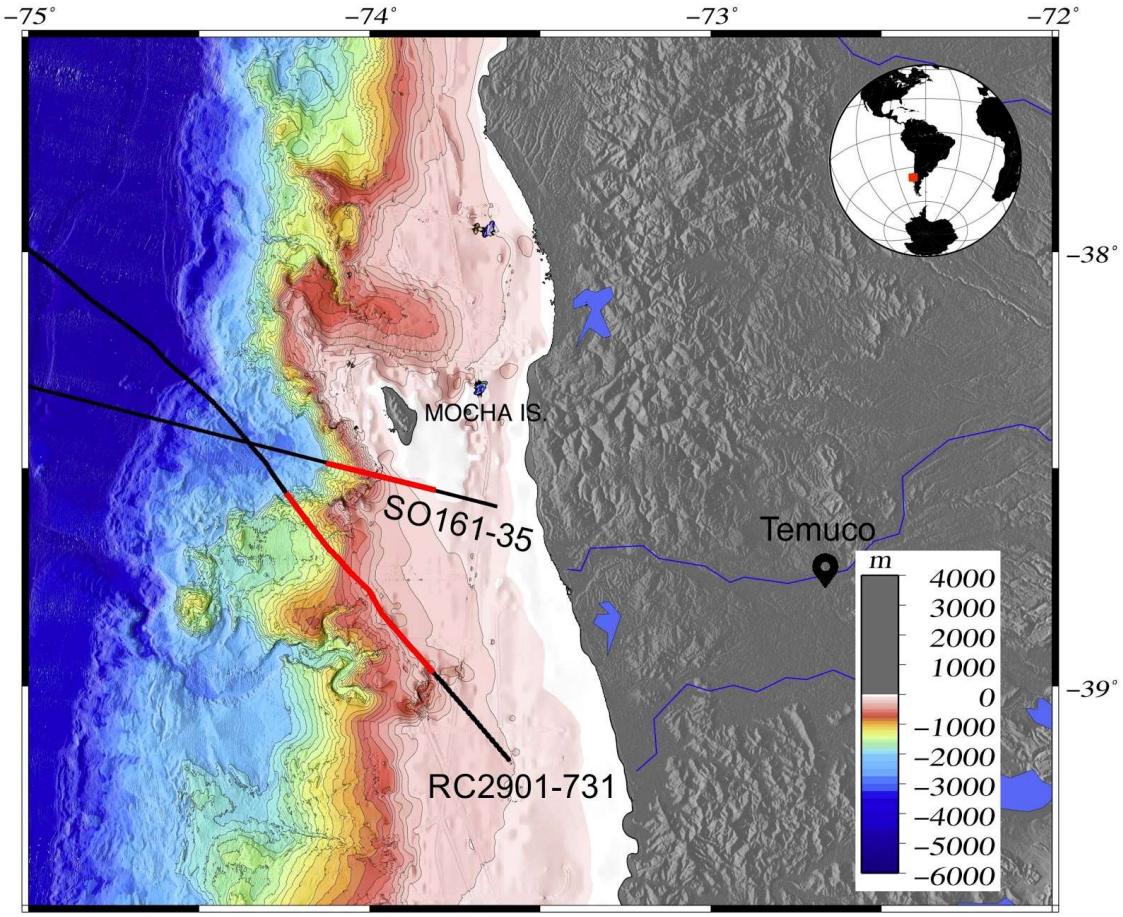

Figure 1. Location map. Red lines indicate the parts of the seismic sections analysed in this study.

2. Materials and Methods

2.1. Seismic Data

RC2901-731 and SO161-35 seismic lines were analysed. Seismic data were acquired during 1988 and 2001 in the framework of ODP (Mid-Ocean Spreading Ridge, Chile Ridge; RC2901-731 seismic line) and SPOC (Subduction Processes off Chile; SO161-35 seismic line) projects, respectively. Seismic acquisition parameters are detailed in Table 1. Open-source Seismic Unix [23] software was used to perform the seismic processing.

Table 1: seismic acquisition parameters

Seismic lines	Research Vessel	Long streamer	Channels	Intertrace	Shot spacing	Airguns/total volume
RC2901-731	RV/Conrad	3000 m	240	12.5 m	50 m	10/61.3 L
SO161-35	RV/Sonne	3000 m	25 108	12.5 m 25 m	50 m	20/54.1 L

2.2. Inversion Modelling

Once identified the BSR along seismic lines, two sections close to 20 km-long were chosen. The seismic analysis uses pre-stack data to perform Kirchhoff depth migration in order to model migration velocity by using an iterative algorithm [24]. The seismic migration analysis builds iteratively the velocity model by using a layer stripping approach [25], in which each layer is modelled in depth. The velocity model is built by selecting continuous reflectors. In our case the seafloor (SF), the horizon 1 (H1), the BSR and the base of the free gas (BGR) were selected. The grid was defined considering a vertical and horizontal spacing equal to 10 and 25 m for RC2901-731 and SO161-35 seismic sections, respectively. The migration velocity analysis uses the output of PSDM to evaluate the reliability of velocity by measuring the flatness in Common Image Gathers (CIGs). At each iteration, the migration velocity analysis is corrected for the purpose of to flat the events in the CIGs; when the events became flats, the velocity layer is fixed and a new horizon is analysed. The number of iterations of each layer necessary to flat the events are detailed in Table 2:

Table 2: Layer iteration numbers

RC2901-731 seismic section		SO161-35 seismic section	
Layers	Iterations	Layers	Iterations
Seawater	3	Seawater	4
From SF to H1	5	From SF to BSR	15
From H1 to BSR	18	Free gas	10
Free gas	4	-	-

A velocity gradient was introduced below the BGR and the final velocity models were smoothed in order to improve the stacked depth migrated image. The stacking of the CIGs was performed by using a maximum offset of 2500 m in order to attenuate stretching effects. Finally, a mixing and band-pass filter was applied; the final sections are shown in Fig. 2.

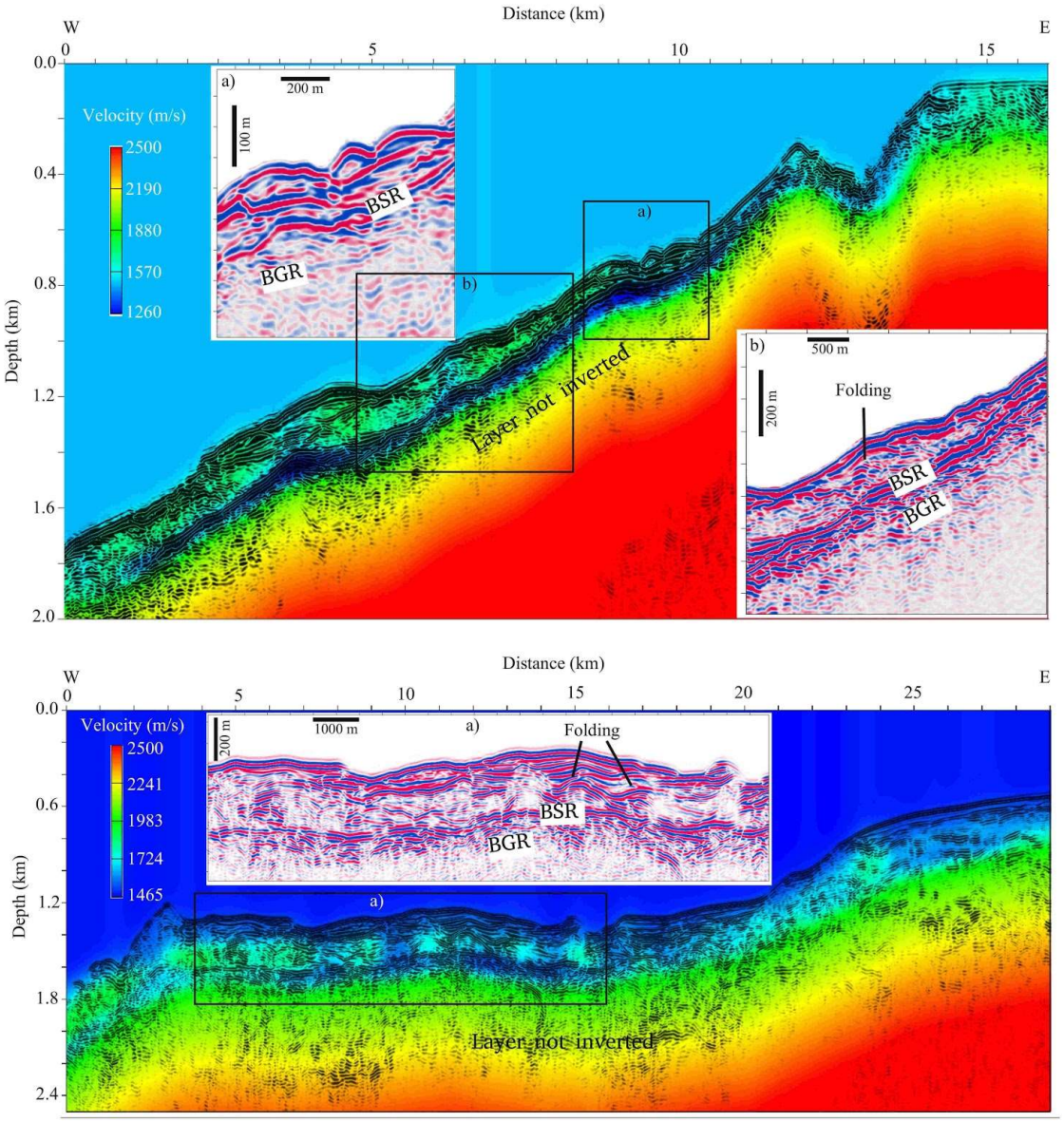

Figure 2. Pre-stack depth sections with superimposed velocity models. Top: SO161-35 seismic section. Bottom: RC2901-731 seismic section. Black boxes indicated with letters show the blow-ups.

2.3 BSR-Derived Geothermal Gradient

It is possible to calculate the geothermal gradient (dT/dZ) by using BSR information, as reported in literature [15,16]. The main parameters to consider are: 1) BSR depth (Z_{BSR}), 2) seafloor depth (Z_{SEA}), 3) BSR temperature (T_{BSR}) and seafloor temperature (T_{SEA}). Thus the geothermal gradient can be obtained by using the following relationship:

$$dT/dZ = (T_{BSR} - T_{SEA})/(Z_{BSR} - Z_{SEA})$$

where T_{SEA} was obtained from ODP information and reported studies in Central Chile [26,27]. The T_{BSR} is based on gas hydrate stability curves reported by [28]. Finally, Z_{BSR} and Z_{SEA} were taken from seismic data analysis.

2.4 Gas phase concentrations

Gas phases (gas hydrates and free gas) concentrations are estimated by using a simplified method [29-31] of the Biot theory [30]. The velocity anomalies (i.e., the difference between the background and seismic velocities) are evaluated considering the geological context in order to associate positive velocity anomalies with gas hydrate concentrations and negative velocity anomalies with free gas concentrations. A qualitative estimate can be obtained by comparing theoretical velocity curves in absence of gas (i.e., the background velocity; [32, 33]) with our seismic velocity curves obtained as described in the section 2.2. The method calculates the free gas concentration in the pore space by considering uniform (gas and water in pore space) and patchy (all gas in patches without water) distributions. In our case, an uniform distribution was considered [30]. Theoretical velocity was modeled by supposing a porosity at the seafloor of 65%, as measured during ODP leg 202 and reported in [27].

3. Results

BSRs were recognized in both seismic sections. Along the whole SO161-35 seismic section the BSR is continuous, strong and shows a variable depth reaching maximum thickness in deepest areas (up to 200 m below seafloor -mbsf; see from 0 to 6 km of distance in Fig. 2), while minimum thickness are located in correspondence to shallowest areas (80 mbsf). On the contrary, RC2901-731 seismic profile shows discontinuous and locally strong BSR, while a constant BSR depths of about 250 mbsf are evidenced from 4 to 16 km of distance (Fig. 2). Note that in this section from 16 to 25 km of distance, the BSR is weak or disappear (Fig. 2). In both sections, the BGR is detected and it is characterized by an average thickness of about 70 m (see blow-up in Fig. 2).

The velocity distribution across SO161-35 and RC2901-731 sections shows strong vertical and lateral variations. The vertical velocity distribution across SO161-35 and RC2901-731 shows a drop below the BSR reaching minimum values of 1260 m/s and 1465 m/s respectively that can be associated to the free gas presence (see Fig. 2). Regarding lateral velocity variations, high velocity values (ranging from 1700 m/s to 1900 m/s) were recognized above the BSRs (Fig. 2). In both sections, faults and fractures with small slips affecting the seafloor were identified in correspondence to low velocity values (Fig. 3). Moreover, in the eastern part of the SO161-35 section a submarine canyon was identified (Fig. 2 and Fig. 3) and a normal fault that configures a lower and upper sector of the RC2901-731 line (see bottom panel of Fig. 3 at 22 km of distance). Finally, in both sections locally dipping reflections were associated to folding (see blow-ups in Fig. 2).

Variable gas hydrate and free gas concentrations were identified, even if the gas hydrate average concentrations are equal to 7.5% of total volume in both sections. On the contrary, the free gas average concentrations are different and equal to 0.4% and 0.12% of total volume in the SO161-35 and RC2901-731 sections respectively. An opposite gas phase concentration trend was observed, in which high gas hydrate concentrations (ranging from 12% to 20% of total volume) overlies to low free gas concentrations (< 0.4% of total volume for RC2901-731 section and < 0.1% of total volume for SO161-35 section), while low gas hydrate concentrations (<4% of total volume in both sections) are in correspondence with high free gas concentrations (up to 1.1 % of total volume for SO161-35 and up to 0.3% of total volume for RC2901-731 sections; see Fig. 3).

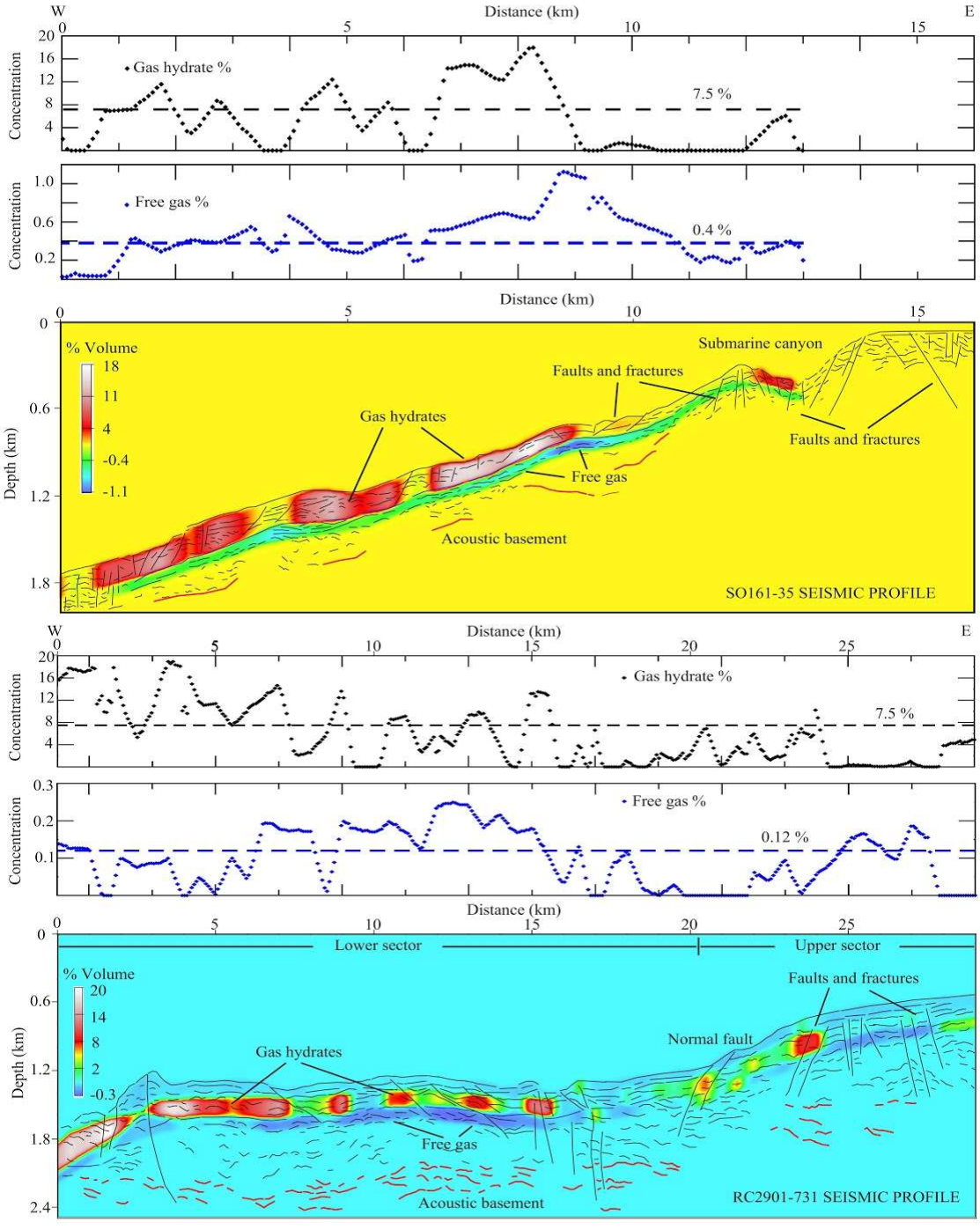

Figure 3. Line drawing sections with superimposed gas phase (gas hydrate and free gas) concentration models. Top three panels: SO161-35 seismic profile. Bottom three panels: RC2901-731 seismic profile. Above each sections are reported gas hydrate (black diamonds) and free gas (blue diamonds) concentration values. Dashed black and blue lines show average values.

A variable geothermal gradient across sections was obtained. However, a recognisable higher geothermal gradient was identified across SO161-35 section (ranging from 60 to 110 °C/km), while lower geothermal gradient across RC2901-731 section was observed (ranging from 35 to 65 °C/km).

The seismic and line drawing sections (Figs. 2 and 3) underline that the lowest geothermal values are located upwards in correspondence with the submarine canyon for SO161-35 section (see Fig. 3 above section at 12 km of distance) and the normal fault for RC2901-731 section (see Fig. 2 below section at 22 km of distance).

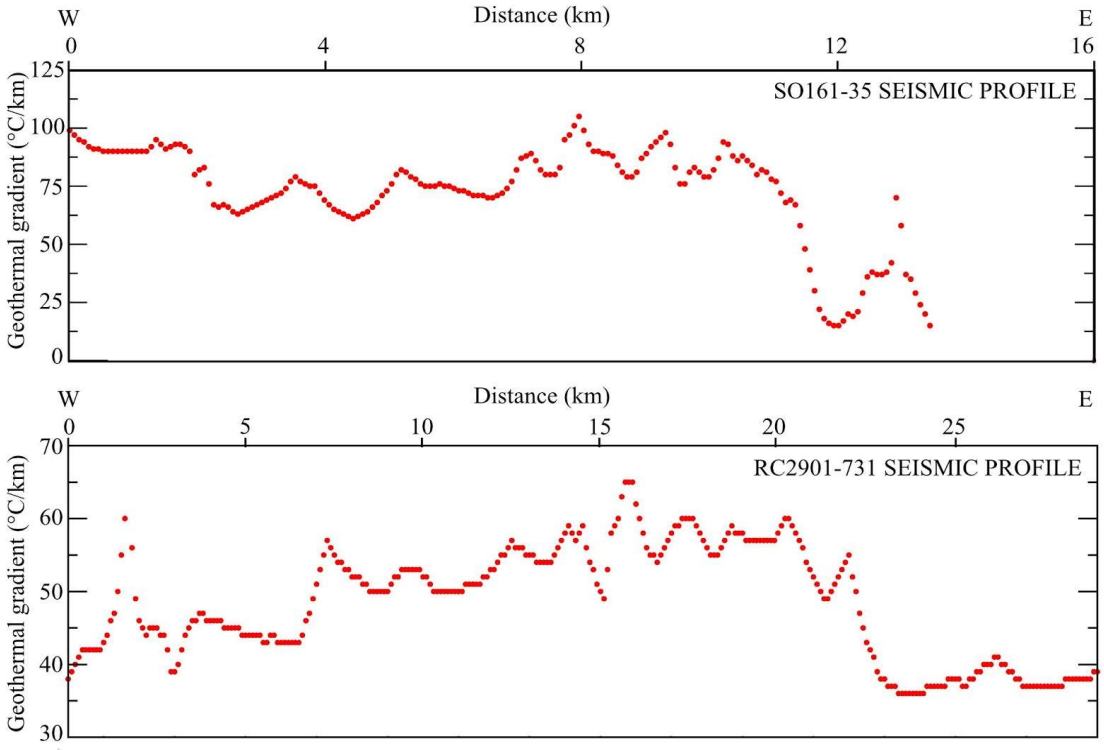

Figure 4. Estimated geothermal gradients. Top: SO161-35 seismic profile. Below: RC2901-731 seismic profile.

4. Discussion

Faults, fractures and folding affecting the shallow sediments in both sections are related to an active domain. In fact, Mocha island is characterised by high seismicity and the uplifting process started during Quaternary [18]. The SO161-35 seismic profile is located approximately 12 km southern Mocha island and shows a strong and continuous BSR, while SO161-731 seismic profile, distant from Mocha island approximately 60 km south, evidences a discontinuous and locally strong BSR. Moreover, a lateral variable BSR depth close to Mocha island (SO161-35 section) was identified, while along RC2901-731 only a slight variation in the BSR depth was recognisable. The BSR seismic character and its depth variability can be related to the gas phase concentrations and the geothermal gradient distribution. Regarding BSR seismic character, several studies argue that strong and continuous BSRs are related to significative free gas concentrations and strong vertical velocity variations [8,34,35]. In our case, across SO161-35 seismic profile the highest free gas concentrations up to 1.1% of total volume (associated to the lowest velocity equal to 1260 m/s) are related to strong vertical velocity variation of 640 m/s, which is the velocity difference between gas hydrate and free gas velocity layers. On the other hand, faraway from Mocha island (RC2901-731 seismic profile), the lowest velocity below BSR increases to 1450 m/s and the difference between gas hydrate and free gas velocities decreases to 400 m/s with respect to the seismic velocity determined in proximity of the Mocha island. The variable depth of the BSR along the SO161-35 section can be explained by a variable geothermal gradient, in which high geothermal gradient values ranging from 60 to 110 °C/km, while a constant BSR depth along the RC2901-731 section could be asociated to low

geothermal gradient values ranging from 35 to 65 °C/km, characterized by a slightly lateral variation. Along the RC2901-731 line, the discontinuous and locally strong seismic character of the BSR can be related with lateral folding presence, in which the gas hydrate and the free gas appear trapped by least across faults and fractures and are highly concentrated at the folding crest. In fact, along this section, areas characterized by high/low velocity above/below the BSR in correspondence to small folding and faults are detected (see RC2901-731 seismic profile in Figs. 2 and 3). Our result is in agreement with several authors that have reported anticlinal structures as structural traps for fluid storing associated to gas hydrate occurrences [12,36-38].

Higher geothermal gradient values were obtained close to Mocha island with average value equal to 85 °C/km against lower geothermal gradient values far off Mocha island with average value equal to 50 °C/km. These results are in agreement with anomalous heat flows reported by [15] in the same area. The former authors argue that the high heat flow variability would be related to ancient sliding processes, in which the headwall slide constitutes a fluid advection zone altering the geothermal gradient at the present. In addition, some authors have proposed this area as a hydrated and/or fluid saturated forearc region [39]. In this context, the fluid supply from deep including gas can be canalised by faults and fractures (Fig. 5) and reaches the hydrate stability zone altering the thermal state giving place to high geothermal gradients as reported in this study. Decreased geothermal gradient faraway from Mocha island is associated with the regional geothermal gradient [15,26,27].

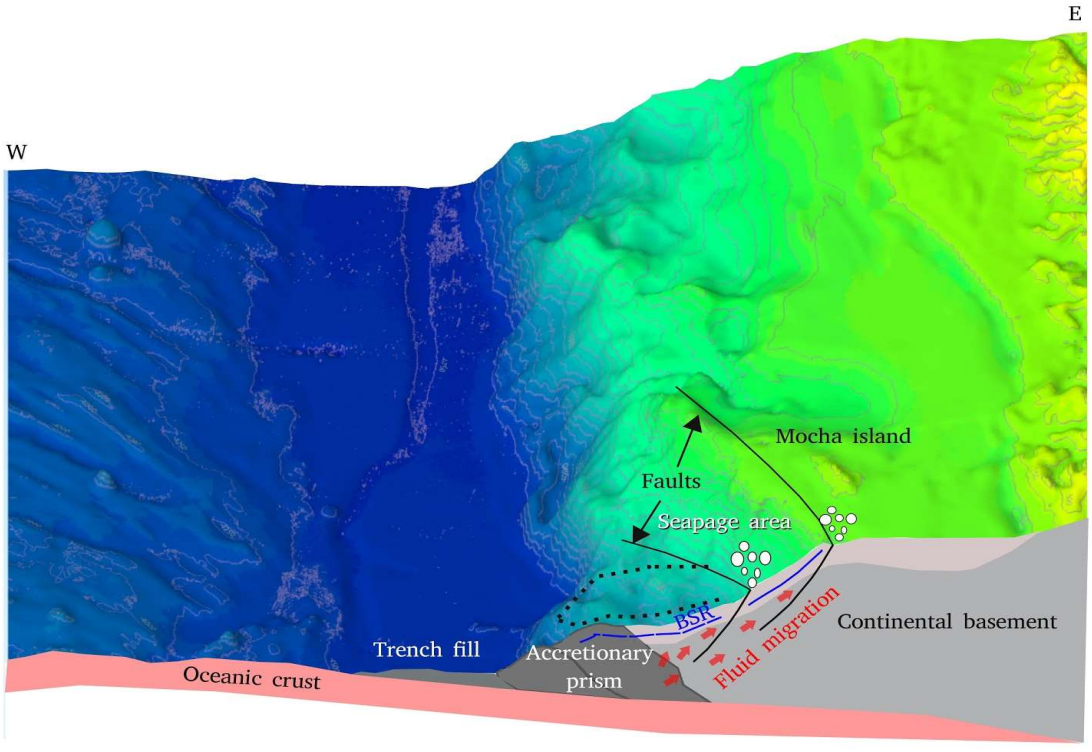

Figure 5. Schematic diagram of SO161-35 seismic profile located close to 38°30'S (see Fig. 1), explaining fluid migration processes close to the Mocha island. Faults are reported by [17,18]. Dashed line shows part of the ancient sliding reported by [40].

High gas hydrate concentrations up to 20% of total volume are reported in both sections, but the highest free gas concentrations up to 1.1% of total volume are located near to the Mocha island (SO161-35 seismic profile), while the lowest free gas concentrations up to 0.3% of total volume are found faraway Mocha island (across RC2901-731 section). In both sections, the highest gas hydrate concentration can be explained as follows: a) high fluid supply from deep zones that can favour gas hydrate formation, as suggested by several authors [15,38] and b) overestimates by compaction due

to deformation processes. On the other hand, the highest free gas concentration located near the Mocha island would be related to the gas hydrate dissociation associated to past sliding processes reported by [40] or free gas stored below an impermeable gas hydrate layer (see Fig. 5), while the lowest free gas concentrations across RC2901-731 seismic line can be explained by lower fluid supply from deep zones and high fluid escape rates preventing free gas storing. These fluid escapes are canalised by faults and fractures affecting seafloor and releasing gas like seeps.

Finally, considering high gas hydrate (average 7.5 % of total volume) and free gas concentrations (0.4 % of total volume) reported in this study, we conclude that close to the Mocha island gas hydrate dissociation processes occurring in the past and, potentially, in the present can constitute the main seepage supply source along this part of the Chilean margin.

Author Contributions: All authors were involved in the data processing and preparation process. All authors were involved in the discussion and revision process with section leads as follows: Iván Vargas-Cordero (Section 1, Section 2, Section 3 and Section 4), Umberta Tinivella (Section 2, Section 3 and Section 4), Lucia Villar-Muñoz and Joaquim P. Bento (Section 3 and 4).

Funding: This research was partially funded by Conicyt, Chile (Fondecyt program), project number 11140216.

Acknowledgments: The authors are very grateful to Joyce Alsop for the seismic data provided at Lamont Doherty Earth Laboratory, USA (LDEO) and V. Damm for the seismic data provided at Federal Institute for Geosciences and Natural Resources, Germany (BGR). We are grateful to CONICYT (Fondecyt de Iniciación N°11140216), which partially supported this work.ts).

Conflicts of Interest: The authors declare no conflict of interest.

References

1. Kvenvolden, K. A. Gas hydrates-geological perspective and global change. Reviews of geophysics 1993, 31(2), 173-187.
2. Bouriak, S.; Vanneste, M.; Saoutkine, A. Inferred gas hydrates and clay diapirs near the Storegga Slide on the southern edge of the Vøring Plateau, offshore Norway. Marine Geology 2000, 163(1-4), 125-148.
3. Bünz, S.; Mienert, J.; Berndt, C. Geological controls on the Storegga gas-hydrate system of the mid-Norwegian continental margin. Earth and Planetary Science Letters 2003, 209(3-4), 291-307.
4. Sultan, N.; Cochonat, P.; Canals, M.; Cattaneo, A.; Dennielou, B.; Haflidason, H.; Urgeles, R. Triggering mechanisms of slope instability processes and sediment failures on continental margins: a geotechnical approach. Marine Geology 2004, 213(1-4), 291-321.
5. Berndt, C.; Mienert, J.; Vanneste, M.; Bünz, S. Gas hydrate dissociation and sea-floor collapse in the wake of the Storegga Slide, Norway. In Norwegian Petroleum Society Special Publications, 2005, 12, 285-292.
6. Horozal, S.; Bahk, J. J.; Urgeles, R.; Kim, G. Y.; Cukur, D.; Kim, S. P.; Kim, J. H. Mapping gas hydrate and fluid flow indicators and modelling gas hydrate stability zone (GHSZ) in the Ulleung Basin, East (Japan) Sea: Potential linkage between the occurrence of mass failures and gas hydrate dissociation. Marine and Petroleum Geology 2017, 80, 171-191.
7. Bangs, N. L.; Sawyer, D. S.; Golovchenko, X. Free gas at the base of the gas hydrate zone in the vicinity of the Chile triple junction. Geology. 1993, 21(10), 905-908.
8. Brown, K. M.; Bangs, N. L.; Froelich, P. N.; Kvenvolden, K. A. The nature, distribution, and origin of gas hydrate in the Chile Triple Junction region. Earth and Planetary Science Letters 1996, 139(3-4), 471-483.
9. Morales, G. Methane hydrates in the Chilean continental margin. Electronic Journal of Biotechnology 2003, 6(2), 80-84.
10. Rodrigo, C.; González-Fernández, A.; Vera, E. Variability of the bottom-simulating reflector (BSR) and its association with tectonic structures in the Chilean margin between Arauco Gulf (37°S) and Valdivia (40°S). Mar. Geophys. Res. 2009, 30, 1-19.
11. Vargas-Cordero, I.; Tinivella, U.; Accaino, F.; Loreto, M. F.; Fanucci, F. Thermal state and concentration of gas hydrate and free gas of Coyhaique, Chilean Margin (44° 30' S). Marine and Petroleum Geology 2010, 27(5), 1148-1156.
12. Vargas-Cordero, I.; Tinivella, U.; Accaino, F.; Loreto, M. F.; Fanucci, F.; Reichert, C. Analyses of bottom simulating reflections offshore Arauco and Coyhaique (Chile). Geo-Marine Letters 2010, 30(3-4), 271-281.

13. Vargas-Cordero, I.; Tinivella, U.; Villar-Muñoz, L.; Giustiniani, M. Gas hydrate and free gas estimation from seismic analysis offshore Chiloé island (Chile). Andean Geology 2016, 43(3), 263-274.
14. Vargas-Cordero, I.; Umberta, T.; Villar-Muñoz, L. Gas Hydrate and Free Gas Concentrations in Two Sites inside the Chilean Margin (Itata and Valdivia Offshores). Energies 2017, 10(12), 2154, doi:10.3390/en10122154.
15. Villar-Muñoz, L.; Behrmann, J. H.; Diaz-Naveas, J.; Klaeschen, D.; Karstens, J. Heat flow in the southern Chile forearc controlled by large-scale tectonic processes. Geo-Marine Letters 2014, 34(2-3), 185-198.
16. Villar-Muñoz, L.; Bento, J. P.; Klaeschen, D.; Tinivella, U.; Vargas-Cordero, I.; Behrmann, J. H. A first estimation of gas hydrates offshore Patagonia (Chile). Marine and Petroleum Geology 2018, 96, 232-239. doi: 10.1016/j.marpetgeo.2018.06.002.
17. Melnick, D.; Echtler, H. P. Inversion of forearc basins in south central Chile caused by rapid glacial age trench fill, Geology 2006, 34(9), 709-712.
18. Melnick, D.; Bookhagen B.; Echtler, H.; Strecker M. Coastal deformation and great subduction earthquakes, Isla Santa Maria, Chile(37°S), Geol. Soc. Am. Bull. 2006, 118(11), 1463-1480, doi:10.1130/B25865.1.
19. Jessen, G. L.; Pantoja, S.; Gutierrez, M. A.; Quinones, R. A.; Gonzalez, R. R.; Sellanes, J.; Hinrichs, K. U. Methane in shallow cold seeps at Mocha Island off central Chile. Continental Shelf Research 2011, 31(6), 574-581.
20. Sellanes, J.; Zapata-Hernández, G.; Pantoja, S.; Jessen, G. L. Chemosynthetic trophic support for the benthic community at an intertidal cold seep site at Mocha Island off central Chile. Estuarine, Coastal and Shelf Science 2011, 95(4), 431-439.
21. Stuardo, J.; Valdovinos, C. A new bathyal Calyptogena from the coast of central Chile (Bivalvia: Vesicomyidae). Venus 1988, 47, 241-250.
22. Tinivella, U.; Loreto, M. F; Accaino, F. Regional versus detailed velocity analysis to quantify hydrate and free gas in marine sediments: the South Shetland Margin case study. Geological Society, London, Special Publications 2009, 319(1), 103-119.
23. Cohen, J.K.; Stockwell, J.W. CWP/SU: Seismic Unix Release 4.0: A free Package for Seismic Research and Processing. Center for Wave Phenomena, Colorado School of Mines: Golden, CO, USA. 2008, 1-153.
24. Liu, Z.; Bleistein, N. Migration velocity analysis: Theory and an iterative algorithm. Geophysics 1995, 60, 142-153.
25. Yilmaz, O. Seismic Data Analysis: Processing, Inversion and Interpretation of Seismic Data. 2nd Edition. Society of Exploration Geophysicists, Oklahoma. 2001, 2027.
26. Grevemeyer, I.; Diaz–Naveaz, J.L.; Ranero, C.R.; Villenger, H.W. Ocean Drilling Program Scientific Party. Heat Flow over the descending Nazca plate in Central Chile, 32° S to 41° S: Observations from ODP Leg 202 and the occurrence of natural gas hydrates. Earth Planet. Sci. Lett. 2003, 213, 285-298.
27. Grevemeyer, I.; Villinger, H. Gas hydrate stability and the assessment of heat flow through continental margins. Geophys. J. Int. 2001, 145, 647-660.
28. Dickens, G.R.; Quinby-Hunt, M.S. Methane hydrate stability in seawater. Geophys. Res. Lett. 1994, 21, 2115–2118.
29. Chand, S.; Minshull, T.A.; Gei, D.; Carcione, J.M. Elastic velocity models for gas hydrate bearing sediments a comparison. Geophysical Journal International 2004, 159, 573-590.
30. Tinivella, U. The seismic response to overpressure versus gas 638 hydrate and free gas concentration. Journal Seismic Exploration 2002, 11, 283-305.
31. Tinivella, U.; Carcione, J.M. Estimation of gas hydrate concentration and free gas saturation from log and seismic data. The Leading Edge 2001, 20, 200-203.
32. Hamilton, E.L. Sound velocity gradients in marine sediments. J. Acoust. Soc. Am. 1979, 65, 909-922.
33. Tinivella, U. A method for estimating gas hydrate and free gas concentrations in marine sediments. Boll. Geofis. Teor. Appl. 1999, 40, 19-30.
34. Hyndman R.D.; Spence G.D. A seismic study of methane hydrate marine bottom simulating reflectors, J. geophys. Res. 1992, 97, 6683-6698.
35. Hovland, M.; Gallagher, J. W.; Clennell, M. B.; Lekvam, K. Gas hydrate and free gas volumes in marine sediments: Example from the Niger Delta front. Marine and Petroleum Geology 1997, 14(3), 245-255.
36. Inks, T.; Lee, M.; Agena, W.; Taylor, D.; Collett, T.; Hunter, T.; Zyrianova, M. Seismic prospecting for gas hydrate and associated free gas prospects in the Milne Point area of northern Alaska. In: Collett, T., Johnson,

A., Knapp, C., Boswell, R. (Eds.), Natural Gas Hydrates – Energy Resource Potential and Associated Hazards. AAPG Memoir, 2009, 89.

37. Loreto, M.F.; Tinivella, U. Gas hydrate versus geological features: The South Shetland case study. Mar. Pet.Geol. 2012, 36, 164-171.

38. Boswell, R.; Rose, K.; Collett, T. S.; Lee, M.; Winters, W.; Lewis, K. A.; Agena, W. Geologic controls on gas hydrate occurrence in the Mount Elbert prospect, Alaska North Slope. Marine and Petroleum Geology 2011, 28(2), 589-607.

39. Haberland, C.; Rietbrock, A.; Lange, D.; Bataille, K.; Dahm, T. Structure of the seismogenic zone of the south central Chilean margin revealed by local earthquake traveltime tomography. Journal of Geophysical Research: Solid Earth 2009, 114(B1).

40. Geersen, J.; Voelker, D.; Behrmann, J. H.; Reichert, C.; Krastel, S. Pleistocene giant slope failures offshore Arauco Peninsula, Southern Chile. J Geol Soc. 2011, 168, 1237-1248.